# Title: Distal axotomy enhances retrograde presynaptic excitability onto injured pyramidal neurons via trans-synaptic signaling

**Authors:** Tharkika Nagendran[1,3], Rebecca L. Bigler[5], Rylan Larsen[2,3], Benjamin D. Philpot[2,3,4], Anne Marion Taylor[1,3,4]*

**Affiliations:**

[1] UNC/NCSU Joint Department of Biomedical Engineering, UNC-Chapel Hill, Chapel Hill, NC 27599 USA

[2] Department of Cell Biology and Physiology, UNC-Chapel Hill, Chapel Hill, NC 27599 USA

[3] Neuroscience Center, UNC-Chapel Hill, Chapel Hill, NC 27599 USA

[4] Carolina Institute for Developmental Disabilities, Chapel Hill, NC 27599 USA

[5] Curriculum in genetics and Molecular Biology Curriculum, UNC-Chapel Hill, Chapel Hill, NC 27599 USA

*To whom correspondence should be addressed: amtaylor@unc.edu

## Abstract

Distal injury of long pyramidal tracts remodels cortical circuitry and leads to enhanced neuronal excitability, thus influencing recovery following injury. The neuron-specific contributions to this retrograde injury-induced hyper-excitability remain unclear due to the complex cellular composition and connectivity of the CNS. We developed a novel microfluidics-based *in vitro* model system to examine intrinsic synaptic remodeling following distal axotomy of long projection pyramidal neurons. We found that distal axotomy of rat pyramidal neurons caused dendritic spine loss at synapses onto the injured neurons followed by a delayed and persistent retrograde trans-synaptic enhancement in presynaptic excitability. Further, this hyper-excitability involved the specific elimination of inhibitory presynaptic terminals formed onto dendritic spines. We found that these changes required differential gene expression and axotomy decreased mRNA expression of the secreted factor netrin-1 coinciding with spine loss. Exogenous netrin-1 applied two days after injury normalized this presynaptic hyper-excitability and restored the fraction of inhibitory inputs onto injured neurons. These findings provide new insights of neuron-specific mechanisms that contribute to synaptic remodeling and demonstrate a novel model system for studying the response of pyramidal circuitry to axotomy.

## Introduction

Brain injury and stroke induce significant synaptic reorganization, even in remote uninjured cortical regions [1-3]. This enhanced neural plasticity allows formation of new connections and expansion of cortical territories, well-described in humans using fMRI and transcranial magnetic stimulation [1, 2, 4, 5], yet the cellular mechanisms of this injury-induced plasticity remain largely unknown.

Long projection pyramidal neurons with somatodendritic domains housed in cortex extend axons into numerous distant areas of the CNS, including the spinal cord and apposing cortical hemispheres. When these remote areas are injured, pyramidal axons are damaged and injury signaling propagates retrogradely to their somatodendritic domains. Retrograde injury signal propagation leads to somatic responses such as chromatolysis and new transcription [6, 7]. After distal spinal cord injury where the corticospinal tract is damaged, spines on the somatodendritic domain of injured pyramidal neurons are lost in cortex [4]. Loss of local GABAergic inhibition also occurs at pyramidal somatodendritic regions following injury, which unmasks preexisting excitatory connections and results in enhanced excitability [2, 8, 9]. These findings suggest that a cascade of events occurs following distal axonal injury involving retrograde axon-to-soma signaling and then trans-synaptic signaling from the injured neuron to uninjured presynaptic neurons causing synaptic changes and enhancing excitability.

Due to the heterogeneity and complexity of the CNS environment, intrinsic neuronal responses to distal axon injury and neuron-specific contributions to synaptic remodeling remain unclear. Reduced preparations are valuable for examining these neuron-specific responses and provide a more experimentally tractable model system to

identify and screen drugs to improve neuronal function following injury. Because brain injury and disease preferentially affects pyramidal neurons [10, 11], we sought to determine the progression of events leading to trans-synaptic changes that occur intrinsically in these neurons following distal axotomy. We overcame the technical challenge of visualizing and manipulating highly polarized and specialized pyramidal neurons using a novel microfluidic approach. We found that distal axotomy of pyramidal neurons led to a delayed trans-synaptic enhancement of presynaptic excitability at synapses onto injured neurons that was transcription-dependent. Further, we identified a trans-synaptic signaling pathway that modulates this axotomy-induced neural plasticity.

## Results

### *In vitro model to study distal axon injury to pyramidal neurons*

To investigate how distal axon injury remodels synapses onto injured neurons, we used a microfluidic approach to compartmentalize pyramidal neurons and subjected them to distal axotomy ~1 mm away from their physically undisturbed dendrites and somata [12, 13]. We used hippocampal neurons to obtain an enriched population of pyramidal neurons. To identify neurons with axons projecting into the axonal compartment, we retrogradely-labeled neurons by applying a G-deleted rabies virus (incompetent for trans-synaptic transfer) to the axonal compartment, and characterized the morphology of the labeled neurons. We found that these neurons were pyramidal (**Figure 1a,b**). Further, axotomized cultures showed no loss in viability post-axotomy (**Figure supplement 1**), similar to *in vivo* findings [14], and injured axons regrew [12, 13]. Supporting the use of this *in vitro* approach, we previously found that axotomy performed within the microfluidic

chambers induced rapid expression of the immediate early gene *c-fos* [13] as also reported *in vivo* [15]. In addition, neurons labeled with retrograde tracer, Alexa 568-conjugated cholera toxin, showed a significant decrease in Nissl staining in the somata reflective of chromatolysis at 24 h post-axotomy [16] (**Figure supplement 1**). Together, this *in vitro* model recapitulated key features of axotomy *in vivo*, and allowed us to examine the response of injured pyramidal neurons far from the site of injury.

*Immature, thin spines are selectively lost after distal axon injury*

Spine loss is seen *in vivo* in models of traumatic brain injury and spinal cord injury [17, 18]. To determine whether similar structural changes occured in cultured pyramidal neurons following distal axotomy, we quantified spine density within the somatodendritic compartment of axotomized neurons that were retrogradely labeled using rabies mCherry virus. Our data showed a significant decline in spine density 24 h and 48 h post-axotomy compared to before axotomy (**Figure 1d** and **Figure supplement 2**). In contrast, control neurons had increased spine density as expected to occur during normal maturation **(Figure 1d and 2e)**. We then analyzed specific spine types that were lost. We found a significant decrease in thin spines, but not stubby spines or mushroom spines, at 24 h post-axotomy compared to pre-axotomy (**Figure 1e**). Further, we found a significant loss of thin and mushroom spines 48 h post-axotomy, (**Figure 1d and 1e**). These results show that distal axon injury triggered persistent loss of thin spines over the course of two days in these neurons.

*A persistent enhancement in synaptic vesicle release rate follows distal injury*

To further evaluate how synapses are modified following distal axon injury, we next investigated whether presynaptic release properties were trans-synaptically altered at synapses onto injured neurons. To address this question we retrogradely infected neurons using a modified eGFP rabies virus to label injured neurons and then used FM dyes to optically measure synaptic vesicle release onto directly-injured neurons (**Figure 2a)**. The use of FM dyes provided us with a non-selective, unbiased method to label a majority of presynaptic terminals within the somatodendritic compartment as described previously [19]. These FM puncta highly colocalized with synapsin1 immunolabeling (93%), validating our FM dye loading strategy (**Figure supplement 3**). We examined the synaptic vesicle release rate of FM puncta that colocalized with eGFP expressing neurons and found that at 24 h post-axotomy there was no measurable change in synaptic vesicle release rate compared to uninjured control samples (**Figure 2b,c**). In contrast, synaptic vesicle release rate was significantly enhanced 48 h after axotomy (**Figure 2c**) and persisted until 4 d post-axotomy. In addition, we found that the FM decay time constant, $\tau$, which has been inversely correlated with release probability [20] was significantly reduced at 48 h post-axotomy (control: 138.3 s ± 8.761 versus axotomy: 88.62 s ± 5.132; $p<0.0001$) and 4 d post-axotomy (control: 222.8 s ± 4.298 versus axotomy: 204.7 s ± 4.126; $p=0.002$). These results were similar to those obtained by examining the entire field of FM puncta rather than selecting only puncta that colocalize with eGFP expressing neurons (**Figure supplement 4**). Together, these data suggest a delayed and persistent increase in synaptic vesicle release rate that occurs following spine loss.

To reconcile our findings of axotomy-induced spine loss and increased presynaptic release, we wondered whether the fraction of responsive presynaptic terminals onto injured neurons increased following axotomy to enhance excitability even though fewer spines are present. We measured the proportion of FM puncta that unloaded (responsive) or did not unload (silent) in response to field stimulation using extracellular electrodes [19] (**Figure 2d**). At 24 h post-axotomy when spine density was decreased, we observed no change in the proportion of responsive and silent FM puncta compared to uninjured controls (**Figure 2d**). However at 48 h post-axotomy, a significantly increased proportion of puncta were responsive compared to uninjured control chambers (**Figure 2d**), suggesting enhanced presynaptic excitability at this time point. Further, at 48 h post-axotomy we found a selective elimination of silent puncta following axotomy while the total number of responsive FM-labeled puncta remained the same (**Figure 2e**). Together, our data suggest that distal axon injury leads to a delayed enhancement in the fraction of responsive presynaptic terminals via the specific reduction of silent puncta.

*Enhanced neurotransmitter release occurs at synapses onto injured neurons*

Our results suggest that distal axotomy triggers a retrograde cascade leading to enhanced presynaptic excitability. To confirm this, we performed electrophysiological recordings of AMPAR-mediated miniature excitatory postsynaptic currents (mEPSCs) from pyramidal neurons within the somatodendritic compartment 48 h post-axotomy compared with age-matched uninjured controls. We noticed a significant increase in mEPSC frequency in axotomized cultures, supporting an increased release rate (**Figure 2f,g**). Membrane properties were equivalent between axotomized and uninjured control

151 neurons supporting the health of these axotomized neurons (**Table supplement 1**).
152 Axotomized cultures also had significantly higher mEPSC amplitudes compared to
153 uninjured controls (**Figure 2g**). This increase in mEPSC amplitude is consistent with our
154 finding that distal axotomy preferentially reduces thin spines over larger-headed spines,
155 which are known to contain more AMPARs [21].

156 Pyramidal neurons extending into the axonal compartment make up 30-50% of
157 neurons within the somatodendritic compartment near the microgrooves (data not
158 shown); thus, not all of the neurons that we recorded were directly injured in the
159 axotomized cultures. We identified whether recorded neurons extended into the axonal
160 compartment by backfilling neurons with biocytin after performing the mEPSC
161 recordings. This allowed us to ask whether the enhanced excitability of presynaptic
162 inputs occured specifically onto injured neurons. Indeed, our data showed that synapses
163 onto directly injured neurons accounted for the changes in both mEPSC frequency and
164 amplitude (**Figure 2h**), while neurons that did not extend into the axonal compartment
165 were not significantly different between the conditions (**Figure 2j**). mEPSC frequency in
166 directly injured neurons showed nearly a two-fold increase compared to the neurons that
167 did not extend axons over to the axonal compartment. Further, these data demonstrate
168 that directly injured neurons retrogradely influenced presynaptic neurotransmitter release
169 through localized synaptic mechanisms that did not affect nearby synapses of uninjured
170 neurons of which mEPSCs were unaffected.

171

*Axotomy selectively eliminates GABAergic terminals onto spines of injured neurons*

Our data show that distal axon injury preferentially eliminated presynaptically "silent" synapses. "Silent" or unresponsive presynaptic terminals may contain glutamate or GABA filled synaptic vesicles [22, 23], thus we next asked whether the eliminated puncta were primarily GABAergic or glutamatergic. We performed retrospective immunostaining to determine the identity of the lost terminals by quantifying the fraction of vGLUT or GAD67-positive FM puncta at 48 h post-axotomy. Interestingly, we found that axotomy did not alter the fraction of glutamatergic terminals (control: 1.00 ± 0.12 versus axotomy: 1.073 ± 0.10; normalized to control), but significantly diminished the fraction of GAD67-positive puncta (Control: 1.00± 0.15 versus axotomy: 0.27 ± 0.07; $p < 0.05$; normalized to control) within the somatodendritic compartment. Thus our data suggest that distal axon injury induced a delayed enhancement in the fraction of responsive presynaptic terminals via a reduction in the number of inhibitory terminals onto injured neurons, and not the number of excitatory presynaptic terminals.

Although the majority of GABAergic synapses are found on dendritic shafts, a minor populations are also found on dendritic spines [24, 25]. Inhibitory synapses formed on dendritic spines allow for compartmentalization of dendritic calcium levels involved in regulation of neuronal activity [26, 27]. To investigate whether dendritic spines receiving inhibitory inputs (i.e., inhibited spines) are lost following axotomy, we quantified the number of inhibitory and excitatory presynaptic terminals onto spines of pyramidal neurons subjected to distal axotomy compared to uninjured controls using retrospective immunostaining for inhibitory (vGAT) and excitatory (vGLUT) synapse markers. We found no significant change in the fraction of vGLUT and vGAT-positive spines at 24 h

post-axotomy (**Figure 3)**. However, we noticed a significant decrease in the fraction of vGAT-positive spines at 48h post-axotomy compared to uninjured control (**Figure 3a,c)** with no significant influence on glutamergic spines. Together, our data suggests that delayed loss of inhibitory synapses on injured neurons alters neuronal activity resulting in an enhancement in presynaptic excitability.

*Altered gene transcription mediates enhanced neurotransmitter release*

To determine whether injury-induced transcription is required for these trans-synaptic changes, we treated the somatodendritic compartment with the reversible transcriptional blocker, DRB, 15 min prior to axon injury and removed the drug 45 minutes later. We found that blocking transcription during this brief time prevented significant changes in the proportion of responsive (**Figure 4b**). Also transcription blockade prevented changes in synaptic vesicle release rate 48 h post-axotomy (**Figure 4c**). However, action potential blockade with TTX in the somatodendritic compartment for ~1 h at the time of injury did not affect injury-induced changes in presynaptic release or the proportion of responsive puncta (**Figure 4d-f**). Further, application of HBS or DMSO as respective vehicle controls to TTX or DRB treatments did not alter injury-induced increase in presynaptic release. We conclude that a transcriptional response is a critical mediator of the delayed trans-synaptic changes in presynaptic release properties following distal axon injury.

*Differential gene expression at 24 h post-axotomy*

Our data show that a transcriptional response was required immediately after axotomy to induce retrograde changes in synaptic vesicle release onto injured neurons. To identify genes that might mediate this process within a longer therapeutically relevant time window, we performed a gene expression study to identify differentially expressed transcripts within the somatodendritic compartment at 24 h post-axotomy compared to uninjured controls. We found 615 transcripts that were significantly changed following injury (one-way between-subject ANOVA, $p < 0.05$) (**Figure 5a; table supplement 1**). Confirming that the transcription response *in vitro* recapitulated *in vivo* findings, we found Jun upregulated 1.41 fold in our microfluidic cultures 24 h post-axotomy [14].

*Netrin-1 mRNA and DCC protein are down-regulated post-axotomy*

To identify potential trans-synaptic mediators that may influence synaptic vesicle release at synapses onto injured neurons, we focused on differentially expressed transcripts that are known to localize to cell-cell contacts, such as synapses (**Figure 5b**). Within this category only 6 transcripts were significantly changed. These transcripts included Podoplanin (Pdpn), Kinesin family member 26B (Kif26b), Cadherin 24 - type2 (Cdh24), Myosin X (Myo10), Netrin1 (Ntn1) and Intercellular adhesion molecule2 (Icam2). We found that netrin-1 was significantly downregulated in our microarray study and this was further confirmed by RNA-sequencing analysis of an additional set of axotomized and uninjured neurons harvested from microfluidic chambers (unpublished data). Netrin-1 is a secreted axon guidance and synaptogenic cue that is enriched at mature dendritic spines [28] and is known to induce synaptic DCC clustering and enhance

239 synapse maturation [29]. Further, loss of secretory or trophic factors are known to induce
240 axotomy-like injury signals [30]. Because of the absence of suitable antibodies for
241 performing netrin-1 immunofluorescence, we tested whether its receptor, DCC, was
242 reduced following axotomy, as DCC levels parallel netrin-1 expression changes [31, 32].
243 While overall expression levels of DCC throughout the somatodendritic compartment
244 were unchanged, we found a significant decrease in local synaptic DCC
245 immunofluorescence at spines of axotomized neurons at 48 h post-injury (**Figure 6b and**
246 **c**). These data suggest that loss of netrin-1 in the somatodendritic compartment of
247 axotomized neurons may contribute to the trans-synaptic changes in neurotransmitter
248 release.

249

250 *Exogenous netrin-1 normalizes injury-induced enhancement in presynaptic excitability*

251 To determine if netrin-1 could normalize the injury-induced enhancement in
252 excitability, we applied exogenous netrin-1 to the somatodendritic compartment 40 h
253 after-injury and evaluated the resulting changes in synaptic vesicle release and
254 responsiveness compared to vehicle control at 48 h after injury. We found that
255 application of exogenous netrin-1 normalized synaptic DCC levels to that of uninjured
256 controls (**Figure 6b and c**). Further, exogenous netrin-1 increased the total number of
257 FM puncta at 48 h post-injury to levels found in the uninjured control (**Figure 6d**). We
258 also observed that application of netrin-1 for 8 h was sufficient to normalize injury-
259 induced changes in the percentage of responsive puncta (**Figure 6e**). Further, netrin-1
260 treatment specifically led to the normalization of the number of silent and inhibitory
261 boutons, GAD67-positive FM puncta, without significantly altering the number of

262 responsive or glutamatergic terminals, vGlut-positive FM puncta (**Figure 6f,g**). Together,
263 our data suggests a novel role for netrin-1 in reducing injury-induced presynaptic hyper-
264 excitability by restoring the excitatory/inhibitory balance.

265

266 **Discussion**

267 We developed a novel model system to examine intrinsic retrograde synaptic
268 remodeling following axon injury that allows unique access to an enriched population of
269 pyramidal neurons. Importantly, this *in vitro* model system recapitulates hallmarks of
270 neurons subjected to axonal injury *in vivo*. These common hallmarks include
271 chromatolysis [6, 16], retrograde spine loss [4, 17, 18], retrograde hyper-excitability [1-3], and
272 disinhibition [2, 8, 9]. In addition, axotomy-induced transcriptional changes in this *in vitro*
273 model are consistent with *in vivo* findings [7, 15]. This *in vitro* model system provides a
274 unique tool to examine axotomy-induced retrograde signaling intrinisic to neurons and
275 the resulting effects to interneuronal communication because of the simplified cellular
276 environment and unprecedented access to neurons for both measurements and
277 manipulations. Our study shows for the first time how changes in intrinsic properties of
278 injured neurons influences presynaptic excitability across cells. This highly reliable *in*
279 *vitro* system will likely be of great benefit for both basic research and drug discovery.

280 Our data show that synapses formed specifically onto directly-injured neurons
281 have altered neurotransmitter release properties. Synapses onto uninjured neurons did not
282 have similar defects, suggesting that the trans-synaptic enhancement in excitability is
283 localized at synapses forming onto injured-neuron during this time. Localized dendritic
284 activity and activity-driven release of secreted proteins (e.g., BDNF, NT-3 and NT-4)

285 from dendrites can trans-synaptically regulate neurotransmitter release [33, 34]. While the
286 mechanisms that locally modulate neurotransmitter release remain unknown, netrin-1
287 signaling presents at least one potential route. Netrin-1 is secreted locally from target
288 cells and signals DCC receptors that are present along axons [29], to influence presynaptic
289 terminal formation and maturation [35, 36].

290 We found a significant reduction in the fraction of inhibitory terminals onto
291 injured neurons 48h post-axotomy. This data together with the persistent loss in spine
292 density post-axotomy, lead us to hypothesize that axotomy induces a specific loss of
293 inhibited spines. Our data showed this was, indeed, the case. This finding is significant
294 because it suggests a new role for the often-ignored inhibitory spines (~10% of spines in
295 our cultures) [24, 25]. It also suggests that excitatory inputs are spared at least for some time
296 following axotomy. Specific loss of inhibitory and not excitatory terminals suggests that
297 retracted excitatory inputs could form new connections while inhibitory ones disappear
298 early after axotomy. It is also possible that large head dendritic spines could receive
299 multiple excitatory inputs suggesting that these terminals are stable and could find new
300 partners over time after injury.

301 Our results showing down-regulation of netrin-1 post-axotomy are consistent with
302 *in vivo* findings following spinal cord injury [37]. Netrin-1 is known to enhance presynaptic
303 terminal formation and maturation [35, 36], thus the loss of netrin-1 following distal injury
304 may have an opposite effect, causing presynaptic terminals to become more functionally
305 immature. Our data supports this conclusion, as we found that presynaptic inputs onto
306 injured pyramidal neurons exhibited a reduced recycling synaptic vesicle pool size and
307 increased release rate, both associated with immature terminals [38, 39]. Further, we found

that application of exogenous netrin-1 normalizes the injury induced decrease in synaptic levels of DCC and the immature-like hyper-excitability (**Figure 6)**. Since netrin-1 and DCC are enriched at glutamatergic synapses within the mature mammalian brain [28], these results point to netrin-1 as a promising therapeutic target to address excitability post-injury. Other trans-synaptic signaling targets (**Figure 5b)** may also influence intrinsic neuronal excitability following brain injury and stroke. Our microfluidics-based model system provides a scalable platform to examine the influence of these and other targets on synaptic remodeling of pyramidal neurons following distal injury.

## Materials and Methods

*Hippocampal cultures.* Dissociated hippocampal cultures were prepared from Sprague Dawley rat embryos (E17-E18) as previously described [13, 19] with the following modifications. Hippocampal tissue was dissected in dissociation media (DM) containing 82 mM $Na_2SO_4$, 30 mM $K_2SO_4$, 5.8 mM $MgCl_2$, 0.25 mM $CaCl_2$, 1 mM HEPES, 20 mM Glucose and 0.001% Phenol red. For enzymatic digestion, equal volumes of TrypLE Express (Invitrogen) and DM were added to the tissue and incubated at 37°C for 8 min. Tissue was then rinsed and gently triturated in neuronal culture media consisting of Neurobasal media (Invitrogen) supplemented with 1x B27 (Invitrogen), 1x Antibiotic-antimycotic (Invitrogen), 1x Glutamax (Invitrogen). Dissociated cells were resuspended in neuronal culture media to yield $12x10^6$ cells per ml.

*Microfluidic chambers.* Poly(dimethylsiloxane) (PDMS) microfluidic chambers were replica molded from microfabricated master molds as described previously [13]. All

experiments used chambers with 900 µm long microgrooves to separate the somatodendritic and axonal compartments as described previously [12, 13, 19]. Microfluidic chambers were placed onto glass coverslips coated with 500-550 kDa Poly-D-Lysine (BD Biosciences). Approximately ~90,000 cells were plated into the somatodendritic compartment and axons extended into the adjacent axonal compartment after 5-7 days of culture. Axotomy was performed at 13 days in vitro (DIV) as described previously [12, 13].

*Retrograde labeling.* Retrograde labeling was performed using either modified cholera toxin or rabies virus. Cholera Toxin Subunit B Alexa Fluor 488 or 568 (Life technologies, Molecular Probes; 1 µg in 200µl of neuronal culture media) was added to the axonal compartment of the microfluidic chamber and incubated for ~ 15h at 37°C. After 15h of incubation, the axonal compartment media was removed, rinsed and replaced using fresh neuronal culture media before performing axotomy or imaging.

G-deleted Rabies-mCherry virus [40] (Salk Institute; $1x10^5$ viral units) in 50 µl-conditioned media was added to the axonal compartment of each chamber and incubated for 2h at 37°C. Conditioned media was added back to the axonal compartments following two washes with fresh NBE media. Chambers were maintained in 37°C incubator for ~48 h until mCherry expression was visible.

*Cell viability assay.* Dead cells were labeled using SYTOX Green (Invitrogen) at a final concentration of 1 µM and all cell nuclei were labeled with NucBlue Hoechst Stain (Invitrogen). Cells were incubated with SYTOX/Hoechst solution simultaneously in 1x PBS for 5 min at 37°C, washed with PBS, and fixed with 4% paraformaldehyde (PFA)

354 in PBS containing 40mg/ml sucrose, 1 µM $MgCl_2$ and 0.1 µM $CaCl_2$ for 15 min at room
355 temperature (RT). Coverslips were then rinsed three times with PBS and mounted onto
356 the glass slide using Fluoromount G (Southern Biotech). SYTOX positive ($Sytox^+$) cells
357 were manually counted in ImageJ using sum projected z-stack confocal images. Percent
358 cell viability is calculated using [($Sytox^+$ - Hoechst) / Hoechst] * 100.
359
360 *Nissl Staining.* Neuronal cultures retrogradely labeled with Cholera Toxin were
361 either axotomized or left uninjured. PDMS chambers were carefully lifted off from PDL
362 coated coverslips 24 h post-axotomy. Cultures on the coverslips were quickly rinsed
363 twice with PBS, fixed with 4% PFA for 30 min at RT, washed twice in PBS, and
364 incubated in 0.1% Triton X-100/PBS for 10 min at RT. Cultures were incubated for 20
365 min in NeuroTrace 500/525 Green Fluorescent Nissl Stain (1:100; Invitrogen) and
366 washed for 10 min in 0.1% Triton X-100/PBS. Cell nuclei were stained with DAPI
367 (Sigma-Aldrich), rinsed three times in PBS, and then the coverslip was mounted onto a
368 microscope slide using Fluoromount G.
369
370 *Immunocytochemistry.* PFA fixed neuronal cultures were permeabilized in 0.25%
371 Triton X-100 and blocked in 10% normal goat serum for 15 min each. Coverslips were
372 incubated with anti-GAD67 (1:2000; Aves labs, GAD), anti-vGLUT1 (1:100;
373 NeuroMab), anti-vGAT (1:1000; Synaptic Systems), anti-DCC (1:100; Calbiochem), or
374 anti-synapsin1 (1:500; Calbiochem) primary antibodies in 1% blocking solution for
375 overnight at 4°C. Coverslips were then incubated with goat anti-rabbit or goat anti-
376 mouse or anti-chicken secondary antibodies conjugated to Alexa-fluorophores (1:1000;

377 Invitrogen) for 1h at RT. Following PBS washes coverslips were mounted onto the glass
378 slide.
379
380 *RNA isolation.* Total RNA from each of 3 axotomized devices and 3 sham
381 manipulated devices (6 total samples) was isolated from the somatodendritic
382 compartment of DIV14 cultures, 24 h after manipulation, using the RNAqueous-Micro
383 Kit (Ambion) according to the manufactures instructions including DNase treatment,
384 with modifications specific to accessing the microfluidic compartment [12]. Briefly, 50 µl
385 lysis solution was added to one somatodendritic well and collected from the other
386 somatodendritic well. Lysate was added to 50 µl of fresh lysis solution and mixed well
387 by careful pipetting. Further RNA purification steps were performed according to
388 the manufacturer's guidelines. Samples were maintained at -80$^{o}$C until prepared for
389 microarray gene expression.
390
391
392 *Microarray analysis.* Quantification of RNA integrity and concentration was
393 confirmed with an Agilent TapeStation 2200 at the UNC Lineberger Comprehensive
394 Cancer Center Genomics Core. Microarrays were processed at the UNC School of
395 Medicine Functional Genomics Core using the Affymetrix GeneChip WT Plus Reagent
396 Kit for cRNA amplification, cDNA synthesis, fragmenting and labeling. Samples were
397 hybridized to Rat Gene 2.0 ST Arrays (Affymetrix). Data analysis was performed with
398 Affymetrix Expression Console software and Affymetrix Transcriptome Analysis
399 Console v2.0 software to compare axotomized cultures to uninjured control samples

using one-way between-subject ANOVA of normalized intensities. We defined our list of significantly changed transcripts as having a fold change absolute value ≥ 1.1 and an ANOVA p-value <0.05. To further identified cell-cell adhesion transcripts by searching for the biological process gene ontology category 'cell-cell adhesion'. Fold-change was calculated by dividing the mean $\log_2$ intensity value of the uninjured control by the mean $\log_2$ intensity value of the axotomized culture samples. The microarray data will be submitted to GEO and accession numbers will be provided at the time of publication.

*Image acquisition and dendritic spine analysis.* High-resolution z-stack montages of mCherry labeled live (60x 1.2 NA water objective) and fixed (60x 1.3 NA silicon oil immersion objective) neurons were captured using Olympus IX81 microscope. To track axotomy induced changes, mCherry labeled 24 h post-axotomy cultures and those uninjured were fixed with 4%PFA for 30 min RT. Dendrite and spine measurements from montages of fixed (**Figure 2- figure supplement 1**) or live neurons were analyzed as described below. In live imaging, we captured "before axotomy" confocal z-stack images using a 60x objective to create montages of neurons extending axons into the axonal compartment. Axotomy was performed on the same day after acquiring these images. Images were acquired from same neuron 24 h post-axotomy. Calibrated z-stack montages were analyzed for all dendrite and spine parameters. Dendrites were traced using semiautomatic neurite tracing tool, Neuron J [41, 42]. Dendrites greater than 10 μm in length were used in the analysis and were quantified for total dendrite length and number of branch points (total number of dendrites - number of primary dendrites). Number of spines on all dendritic segments of each neuron were manually labeled and categorized as

thin, stubby or mushroom shaped based on each spine's head to neck diameter ratio (neck ratio) and length to head diameter ratio using Neuron studio [43]. Spine density was calculated for 10 µm length of dendrite as [(# of spines / total dendrite length)*10].

*FM dye experiments and analysis.* Cultures in microfluidic chambers at 24 h (14DIV), 48 h (15DIV), and 4d (17DIV) post-axotomy were loaded with lipophilic dye FM® 5-95 (Invitrogen) using KCl mediated depolarization as described previously [19]. Briefly, culture were first incubated for 30 min with pre-warmed HEPES-buffered solution (HBS; 119 mM NaCl, 5 mM KCl, 2 mM $CaCl_2$, 2 mM $MgCl_2$, 30 mM glucose, 10 mM HEPES). Media was then replaced with FM dye loading solution containing 10 µM FM 5-95, 20 µM AMPAR antagonist 6-cyano-7-nitroquinoxaline-2,3-dione disodium (CNQX; Tocris), 50 µM NMDAR antagonist D-(-)-2-amino-5-phosphonopentanoic acid (D-AP5; Tocris) in 90 mM KCl HBS for 1 min. The loading solution was replaced with HBS containing 10 µM FM 5-95 for 1 min and later rinsed three times with a high-$Mg^{2+}$, low-$Ca^{2+}$ solution (106 mM NaCl, 5 mM KCl, 0.5 mM $CaCl_2$, 10 mM $MgCl_2$, 30 mM glucose, 10 mM HEPES) containing 1 mM Advasep-7 (Biotium) to remove extracellular membrane-bound FM. Finally, cultures were washed in HBS containing 20 µM CNQX and 50 µM D-AP5 for at least three times, 1 min each. Next, we stimulated the microfluidic chambers using extracellular electrodes by placing a positive and negative electrode in each well of the somatic compartment.

Electrical stimulation was provided by an AD Instrument 2 Channel Stimulus Generator (STG4002) in current mode with an asymmetric waveform (-480 µA for 1 ms and +1600 µA for 0.3 ms) for ~ 1 min at 20 hz for 600 pulses. Z-stacks (31 slices) were

captured every 15s. This stimulation pattern was optimized for efficient FM unloading within these microfluidic chambers and the frequency is greater than typically used in open well dishes. At least 3 baseline images were acquired before electrical stimulation. Sum projected confocal z-stack were converted to 8-bit images and registered using TurboReg, an image J plugin. We background subtracted the image stack using the image 3 min after stimulation. The image stack thresholded to a pixel value of 15. FM puncta between 2 to 50 (pixels^2) were analyzed. We measured the intensity of each punctum in the whole field or specifically on GFP labeled neuron (**fig. 3a-c**) throughout all time-series (registered stack obtained by TurboReg, imageJ plugin). To analyze the unloading kinetics of FM puncta on GFP labeled neuron, we first thresholded the GFP image and then created an outline enclosing all the GFP labeled regions including spines. The outlined ROI was superimposed on the FM labeled image and the intensity of each punctum in the selected ROI (GFP outline) was measured throughout all time series. We normalized fluorescent intensity of each puncta to the frame before stimulation. Puncta with >5% unloading after 1 min were used in the analysis as unloaded puncta. Time constants were estimated by curve fitting unloading kinetics to a single exponential decay function [19]. Curve fitting was done in MATLAB. Number of FM puncta that unload >5% after 60s were classified as responsive using image stacks that were not background subtracted; pucnta that did not meet this criteria were classified as silent or unresponsive.

In activity and transcription blocking experiments, Tetrodotoxin citrate (TTX; Tocris Bioscience) was suspended in HBS and 5,6-dichloro-1-β-D-ribofuranosyl-1H-benzimidazole (DRB; Sigma-Aldrich) was suspended in DMSO (**Figure 4)**. The FM 5-95

469 unloading experiment was performed as mentioned above at 48 h post-axotomy. The
470 intensity measurements of each punctum in the whole field and subsequent analysis of
471 FM unloading kinetics was peformed as mentioned above.
472
473 *Microscopy.* Images were captured using CSU-X1 spinning disk confocal imaging
474 unit configured for an Olympus IX81 microscope (Andor Revolution XD). The FM 5-95
475 imaging was performed as described previously [19]. Z-stack images were acquired every
476 15s during the baseline (1 min), stimulation (1 min), and after stimulation (2 min)
477 periods.
478
479 *mEPSCs Recordings.* AMPAR-mediated mEPSC recordings were performed
480 similar to previously described [44]. For whole-cell recordings, neurons were visually
481 identified with infrared differential interference contrast optics. Cells were recorded in
482 voltage-clamp configuration at -70 mV with a patch clamp amplifier (Multiclamp 700A,
483 Molecular Devices). Data were acquired and analyzed using pCLAMP 10 software
484 (Molecular Devices). Series and input resistances were monitored throughout the
485 experiments by measuring the response to a −5-mV step at the beginning of each sweep.
486 Series resistance was calculated using the capacitive transient at the onset of the step and
487 input resistance was calculated from the steady-state current during the step. Recordings
488 were sampled at 10 kHz and bessel filtered at 2 kHz. No series resistance compensation
489 was applied.
490 Microfluidic chambers, PDMS molds, were removed and the glass coverslips
491 containing cells were mounted onto a submersion chamber, maintained at 32º C. Cultures

were perfused at 2 mL/min with artificial cerebrospinal fluid (ACSF) containing 124 mM NaCl, 3 mM KCl, 1.25 mM $Na_2PO_4$, 26 mM $NaHCO_3$, 1 mM $MgCl_2$, 2 mM $CaCl_2$ and 20 mM d-(+)-glucose, saturated with 95% $O_2$, 5% $CO_2$. AMPAR-mediated mEPSCs were isolated by supplementing ACSF with TTX citrate (1 μM, Abcam), the GABA (A) receptor antagonist picrotoxin (50 μM, Sigma-aldrich), and the NMDA receptor antagonist D, L-2-amino-5 phosphonopentanoic acid (100 μM, AP5, Abcam). Open tip resistances were between 2-5 MΩ when pipettes were filled with internal solution containing: 100 mM $CsCH_3SO_3$, 15 mM CsCl, 2.5 mM $MgCl_2$, 5 mM QX-314-Cl, 5 mM tetra-Cs-BAPTA, 10 mM HEPES, 4 mM Mg-ATP, 0.3 mM Na-GTP, and 0.5% (w/v) neurobiotin with pH adjusted to 7.25 with 1 M KOH and osmolarity adjusted to ~295 mOsm with sucrose. To determine if recorded neurons' axons entered the microfluidic chamber, 0.035 Alexa-594 was also included in the internal solution to allow for post-hoc visualization of neuronal morphology.

Events with a rapid rise time and exponential decay were identified as mEPSCs using an automatic detection template in pCLAMP 10, based on previously published methods [45]. Events were post-hoc filtered to only include events with a peak amplitude ≥5 pA and a ≤3 ms 10-90% rise time. Mean mEPSC parameters were quantified from a 10 min recording period. Neurons were excluded from analysis if $R_{series}$ was ever >20 MΩ during anytime during the recording.

*Statistics.* Graphpad prism 6 statistical program was used. For calculating significance on spine density in live imaging data, paired two-tailed t-test was performed. Unpaired two-tailed t-test was performed when comparing two groups. For FM

unloading experiments and for comparing multiple groups, Two-way ANOVA and One-way ANOVA were used respectively followed by Bonferroni post-hoc test.

**References:**

1. Nudo, R.J. *Front Hum Neurosci* 7, 887 (2013).
2. Takechi, U., *et al. Clin Neurophysiol* 125, 2055-2069 (2014).
3. Nudo, R.J. & Milliken, G.W. *J Neurophysiol* 75, 2144-2149 (1996).
4. Oudega, M. & Perez, M.A. *J Physiol* 590, 3647-3663 (2012).
5. Frost, S.B., *et al. J Neurophysiol* 89, 3205-3214 (2003).
6. Rishal, I. & Fainzilber, M. *Nat Rev Neurosci* 15, 32-42 (2014).
7. Urban, E.T., 3rd, *et al. Molecular and cellular biochemistry* 369, 267-286 (2012).
8. Jacobs, K.M. & Donoghue, J.P. *Science* 251, 944-947 (1991).
9. Ding, M.C., *et al. J Neurosci* 31, 14085-14094 (2011).
10. Nakatomi, H., *et al. Cell* 110, 429-441 (2002).
11. Will, B., *et al. Progress in Neurobiology* 72, 167-182 (2004).
12. Taylor, A.M., *et al. J Neurosci* 29, 4697-4707 (2009).
13. Taylor, A.M., *et al. Nat Methods* 2, 599-605 (2005).
14. Greer, J.E., *et al. J Neurosci* 32, 6682-6687 (2012).
15. Ikeda, S. & Nakagawa, S. *Brain Res* 792, 164-167 (1998).
16. McIlwain, D.L. & Hoke, V.B. *BMC Neurosci* 6, 19 (2005).

17. Ghosh, A., *et al. Cereb Cortex* 22, 1309-1317 (2012).

18. Gao, X., *et al. PLoS One* 6, e24566 (2011).

19. Taylor, A.M., *et al. J Neurosci* 33, 5584-5589 (2013).

20. Zakharenko, S.S., *et al. Nat Neurosci* 4, 711-717 (2001).

21. Matsuzaki, M., *et al. Nat Neurosci* 4, 1086-1092 (2001).

22. Li, P. & Zhuo, M. *Nature* 393, 695-698 (1998).

23. Bekkers, J.M. *J Neurosci* 25, 4031-4039 (2005).

24. Chen, J.L., *et al. Neuron* 74, 361-373 (2012).

25. Markram, H., *et al. Nat Rev Neurosci* 5, 793-807 (2004).

26. Chiu, C.Q., *et al. Science* 340, 759-762 (2013).

27. Higley, M.J. *Nat Rev Neurosci* 15, 567-572 (2014).

28. Horn, K.E., *et al. Cell Rep* 3, 173-185 (2013).

29. Goldman, J.S., *et al. J Neurosci* 33, 17278-17289 (2013).

30. Shadiack, A.M., *et al. J Neurosci* 21, 363-371 (2001).

31. Xu, K., *et al. Science* 344, 1275-1279 (2014).

32. Manitt, C., *et al. J Neurosci* 29, 11065-11077 (2009).

33. Wong, Y.C. & Holzbaur, E.L. *J Neurosci* 34, 1293-1305 (2014).

34. Branco, T., *et al. Neuron* 59, 475-485 (2008).

35. Stavoe, A.K. & Colon-Ramos, D.A. *The Journal of Cell Biology* 197, 75-88 (2012).

555 36. Colon-Ramos, D.A., *et al. Science* 318, 103-106 (2007).

556 37. Manitt, C., *et al. J Neurosci Res* 84, 1808-1820 (2006).

557 38. Blue, M.E. & Parnavelas, J.G. *Journal of neurocytology* 12, 697-712 (1983).

558 39. Bolshakov, V.Y. & Siegelbaum, S.A. *Science* 269, 1730-1734 (1995).

559 40. Wickersham, I.R., *et al. Neuron* 53, 639-647 (2007).

560 41. Fu, M.M. & Holzbaur, E.L. *Autophagy* 10, 2079-2081 (2014).

561 42. Nagendran, T. & Hardy, L.R. *Neuroscience* 199, 548-562 (2011).

562 43. Rodriguez, A., *et al. PLoS One* 3, e1997 (2008).

563 44. Larsen, R.S., *et al. Neuron* 83, 879-893 (2014).

564 45. Clements, J.D. & Bekkers, J.M. *Biophys J* 73, 220-229 (1997).

565

566 **Acknowledgements:** We thank Stephanie Gupton for netrin-1, Kelly Carstens for

567 preliminary gene expression work, and Cassie Meeker for technical support. We thank

568 Randolph Nudo (KUMC), Richard Segal (MUSC), Julius Dewald (RIC) and Taylor lab

569 members for their advice and discussions. **Funding:** R.L.B. was supported in part by a

570 grant from the National Institute of General Medical Sciences under award 5T32

571 GM007092. A.M.T. acknowledges support from the Eunice Kennedy Shriver NICHD

572 (K12HD073945) and the NIMH (R41MH097377). A.M.T. is an Alfred P. Sloan

573 Research Fellow. **Author contributions:** T.N. designed and performed experiments and

574 wrote the manuscript. R.L.B. designed and performed experiments. R.L. designed and

575 performed experiments. B.D.P. designed experiments. A.M.T. designed experiments and

576 wrote the manuscript. **Competing financial interests:** Yes there is potential competing
577 interest. A.M.T. is an inventor of the microfluidic chambers (US 7419822 B2) and has
578 financial interest in Xona Microfluidics, LLC. T.N., R.B., R.L., and B.D.P. declare no
579 competing financial interests.
580

**Figure 1: Distal axotomy of pyramidal neurons within microfluidic chambers induces dendritic spine loss on axotomized neurons.** (**a**) 14 DIV rat hippocampal neurons cultured within a microfluidic chamber. Neurons are retrogradely labeled using a G-deleted rabies mCherry virus added exclusively to the axonal compartment. (**b**) The virally-labeled neurons are pyramidal neurons (94%; 42 of 45 were pyramidal; remaining were unclassifiable). G-deleted rabies mCherry virus labels entire dendritic arbor including spines (Insert). Scale bars, 100 µm. (**c**) Cartoon illustration of *in vitro* axotomy within microfluidic chambers which axotomizes a subset of neurons (red) that extend their axons through the microgrooves. Axons of uninjured neurons (grey) are housed within the somatodendritic compartment. (**d**) Representative images of dendritic segments, retrogradely labeled with G-deleted rabies-mCherry virus, from repeated live imaging of mock injured control and axotomized neurons before and 24 h post-axotomy. Scale bars, 10 µm. Quantification of spine density in live uninjured controls, 24 h post-axotomy and 48 h post-axotomy. Two-tailed t-test, **$p \leq 0.01$. (**e**) Distribution of spine categories in live uninjured controls (before: black open bars; 24 h after: black solid bars), 24 h post-axotomy (before; blue open bars; 24 h after: blue solid bars) and 48 h post-axotomy (before; red open bars; 48 h after: red solid bars). Two-way ANOVA, Bonferroni post hoc test,* $p < 0.05$, ** $p < 0.01$, *** $p < 0.001$; n=6 live neurons per condition from two independent experiments. The same trend was observed in each independent experiment. Error bars, SEM.

**Figure 2: Distal axotomy induces a delayed trans-synaptic increase in presynaptic-excitability onto axotomized neurons.**

(**a**) Representative image of a neuron retrogradely labeled with a modified eGFP rabies virus, within the somatodendritic compartment of a microfluidic chamber. An enlarged region shows colocalization of FM puncta with eGFP-labeled dendrites and dendritic spines (arrows). FM puncta were visualized using the ImageJ 'fire' color look up table shown in *(b)*. Scale bars, 20 µm. (b) Representative images show FM puncta before and after field stimulation. Boundaries of eGFP labeled dendrites and spines are outlined as gray dashed lines. Arrows in the before and after stimulation images indicate destaining of FM labeled puncta in the dendritic spines. The ImageJ color look up table 'fire' was used. Scale bars, 10 µm. (**c**) FM unloading curves from FM puncta colocalized onto GFP labeled neurons at 24 h (control, n=125 puncta combined from 3 chambers; axotomy, n=156 puncta combined from 3 chambers) and 48 h post-axotomy (control, n=150 puncta combined from 3 chambers; axotomy, n=200 puncta combined from 3 chambers). Two-way ANOVA, ***$p \leq 0.001$. Insert: decay time constant ($\tau$) of FM puncta at 24 h and 48 h post-axotomy. Two-tailed t-test, ***$p < 0.001$. Data shown represent two independent experiments. (**d**) Percent of responsive FM puncta and silent FM puncta at 24 h (control, n=1,431; axotomy, n=1,602; data shown is from two independent experiments which includes a total of 4 chambers for each condition) and 48 h post-axotomy (control, n=3,452; axotomy, n=2,793; data shown is from three independent experiments to yield a combined 7 chambers for each condition). Asterisks indicate that the percentage of responsive and silent puncta at 48 h post-axotomy is significantly different from control. Two-tailed t-test, *$p < 0.05$. (**e**) Total number of responsive and silent FM puncta at 48 h

627 post-axotomy (Responsive: control, n=1,536; axotomy, n=1,522; Silent: control,
628 n=1,504; axotomy, n=742; data shown represents three independent experiments which
629 combined included 6 chambers for each condition) Two-tailed t-test, *p< 0.05. (**f**)
630 Representative traces of mEPSC recordings 48 h post-axotomy. (**g**) Quantification of
631 mEPSC frequency and amplitude at 48 h post-axotomy (control, n=17 neurons; axotomy,
632 n=16 neurons). Data shown are combined from three independent experiments. (**h.i**)
633 Subset analysis of mEPSC frequency and amplitude for neurons from (g) that extended
634 axons (*h*; control, n=7 neurons; axotomy, n=9 neurons) or did not extend axons into the
635 axonal compartment (*i;* control, n=10 neurons; axotomy, n=7 neurons). Insert: Cartoon
636 depicts recording from either directly injured neuron (*h*; red) or its neighboring uninjured
637 neuron (*i*; grey). Error bars, SEM. One-tailed t-test, *p< 0.05. The same trend was
638 observed in each independent experiment described above.
639
640

641 **Figure 3: Distal axotomy induces selective loss of inhibited spine synapses onto**
642 **injured neurons.**
643 (**a**) Representative dendritic segments (retrogradely labeled with GFP) showing spines
644 that are labeled with either vGLUT (red) or vGAT (purple) antibodies. White open circles
645 highlight dendritic spines with vGLUT and/or vGAT synapses. (b) Fraction of vGlut
646 positive dendritic spines at 24 h and 48 h post-axotomy normalized to respective controls.
647 (c) Fraction of vGAT positive dendritic spines at 24 h and 48 h post-axotomy normalized
648 to respective controls. 8 individual fields were analyzed per condition from two
649 independent experiments. The same trend was observed in each experiment. Scale bars, 5
650 µm. Two-tailed t-test, ***$p \leq 0.001$. Error bars, SEM.
651
652

**Figure 4: Injury-induced gene transcription is required for enhanced synaptic vesicle release following axotomy.**

(**a**) Experimental timeline illustrating application of transcription blocker (DRB, 80 µM) to the somatodendritic compartment for 1 h prior to and during injury. (**b**) Percent of unloaded FM puncta (responsive) and unresponsive (silent) puncta at 48 h post-axotomy. Approximately 300 puncta were analyzed per chamber; 4 individual chambers were analyzed per condition over two independent experiments. (**c**) FM5-95 unloading following application of DRB. Approximately 200 puncta were analyzed per chamber; 4 individual chambers were analyzed per condition over two independent experiments. (**d**) Experimental timeline illustrating application of action potential blocker (TTX, 1 µM) to the somatodendritic compartment prior to and during injury. (**e**) Percent of unloaded FM puncta (responsive) and unresponsive (silent) puncta at 48 h post-axotomy. Approximately 400 puncta were analyzed per chamber; 4 individual chambers were analyzed for each condition over two independent experiments. Asterisks indicate that the percentage of responsive and silent puncta is significantly different compared to control. Two-tailed t-test, *$p < 0.05$. (**f**) FM5-95 unloading curves following application of TTX. Approximately 200 puncta were analyzed per chamber; 4 individual chambers were analyzed for each condition over two independent experiments). The same trend was observed in each pair of experiments. Two-tailed t-test, **$p < 0.01$. Error bars, SEM.

673 **Figure 5: Differentially expressed transcripts that are critical for synaptic function,**
674 **are altered in the somatodendritic compartment of axotomized neurons.**
675 Microarray analysis was performed on somatodendritic samples of controls and 24 h
676 post-axotomy cultures. (A) Volcano plot showing differentially expressed RNAs that are
677 significantly changed at 24 h post-axotomy (p-value < 0.05; n = 3 individual chambers
678 each condition; **Table supplement 2**). (B) Volcano plot showing differential expression
679 of transcripts from Gene Ontology biological process category “cell-cell adhesion”. Only
680 6 transcripts are significantly changed in this category. Netrin-1 regulates trans-synaptic
681 effects and is significantly down regulated 24 h post-axotomy. One-way ANOVA, p-
682 value < 0.05 represents the transcripts that are consistently changed in each of the three
683 microarray datasets.
684
685

**Figure 6: Netrin-1 treatment normalizes presynaptic hyper-excitability and inhibitory fraction following distal axotomy.**

(**a**) Experimental timeline. (**b**) Representative images of fixed dendritic segments, retrogradely labeled with G-deleted rabies-mCherry virus and immunostained with DCC antibody following exogenous netrin-1 (625ng/ml) treatment. Regions of interest (ROI's; white circles) show synaptic DCC levels at 48 h post-axotomy. Scale bar, 10µm. (**c**) Quantification of DCC fluorescence intensity at 48 h post-axotomy and in response to exogenous application of netrin-1 (control, n=185 ROIs; axotomy, n=165 ROIs; axotomy + netrin-1, n=100 ROIs). At least 4 individual chambers were analyzed per condition from two independent experiments. The same trend was observed in each independent experiment. Two-way ANOVA, Bonferroni post hoc test,***$p < 0.001$. (**d**) Average number of responsive and silent FM puncta per field in response to exogenous application of netrin-1 48 h post-axotomy. Approximately 400 puncta were analyzed per chamber from 7 individual chambers for each condition. Data shown was from two independent experiments and a similar trend was observed in each these experiment. One-way ANOVA, Bonferroni post hoc test, *$p < 0.05$. Noticeably, injury decreased the number of silent FM puncta that was normalized in response to exogenous application of netrin-1 48 h post-axotomy. (**e**) The percent of responsive FM puncta (unloaded puncta) following exogenous application of netrin-1 48 h post-axotomy. Two-tailed t-test, *$p < 0.05$. (**f**) Fraction of vGlut1-positive FM puncta following exogenous netrin-1 application, normalized to vehicle (HBS) controls. (**g**) Fraction of GAD67-positive FM puncta following exogenous netrin-1 application, normalized to vehicle (HBS) controls. (**f,g**) A minimum of 1000 puncta from 6 individual fields was analyzed per condition

over two experiments. The same trend was observed in each independent experiment.

Two-tailed t-test, *$p < 0.05$. Error bars, SEM.

711 **Supplemental figures and tables:**

712 **Figure supplement 1:** Distal axotomy of pyramidal neurons induces dissolution of Nissl
713 substance without affecting cell viability.

714 **Figure supplement 2:** Dendrites retract, show fewer branch points and spines 24 h post-
715 axotomy compared to uninjured controls.

716 **Figure supplement 3:** FM puncta highly colocalizes with synapsin1 labeling.

717 **Figure supplement 4:** FM unloading curves from somatodendritic compartments of
718 microfluidic chambers without rabies virus infection.

719 **Table supplement 1:** Membrane properties of uninjured controls vs. axotomized neurons
720 48 h post-axotomy.

721 **Table supplement 2:** List of transcripts that were significantly changed 24 h after injury.

722

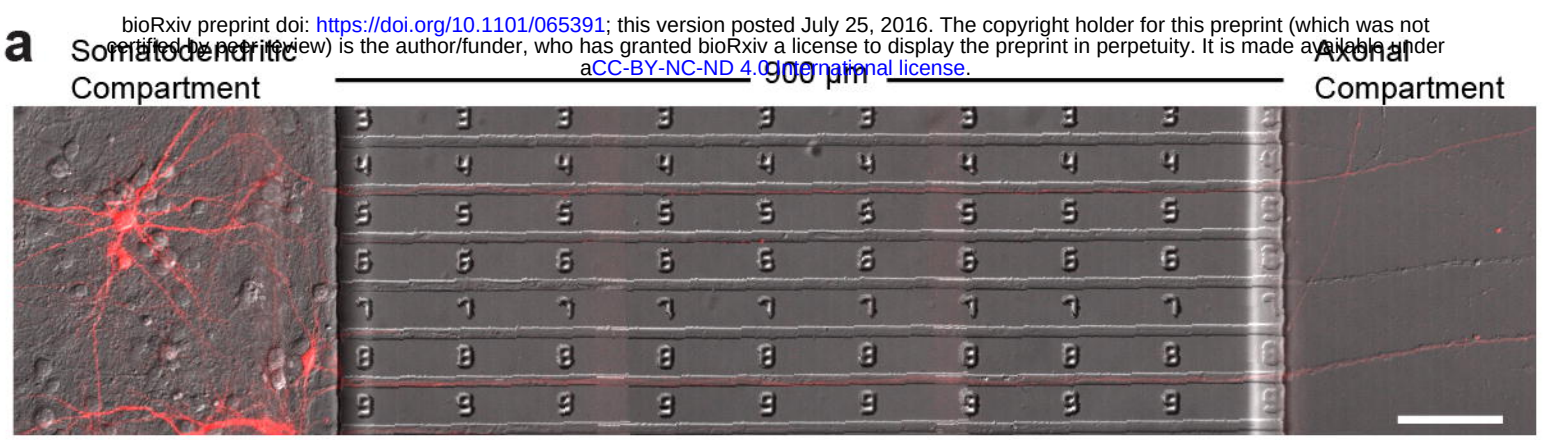


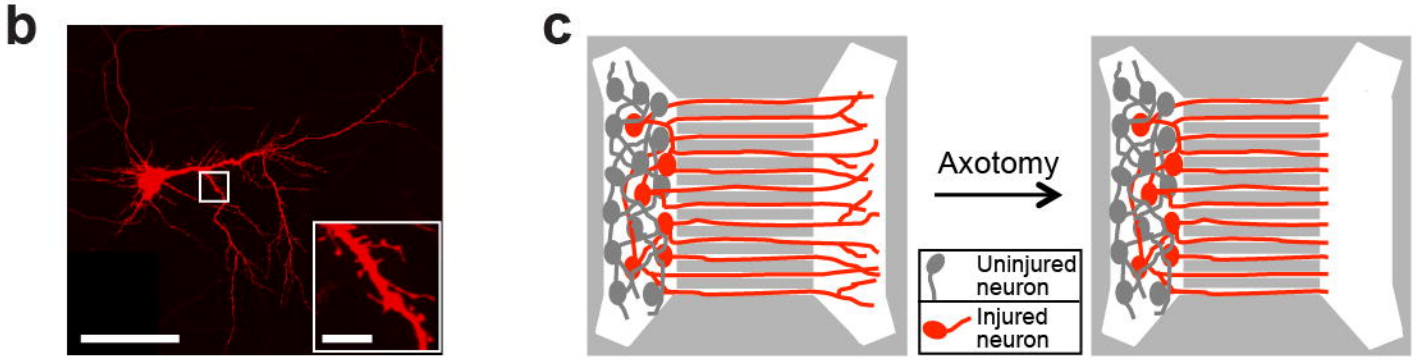


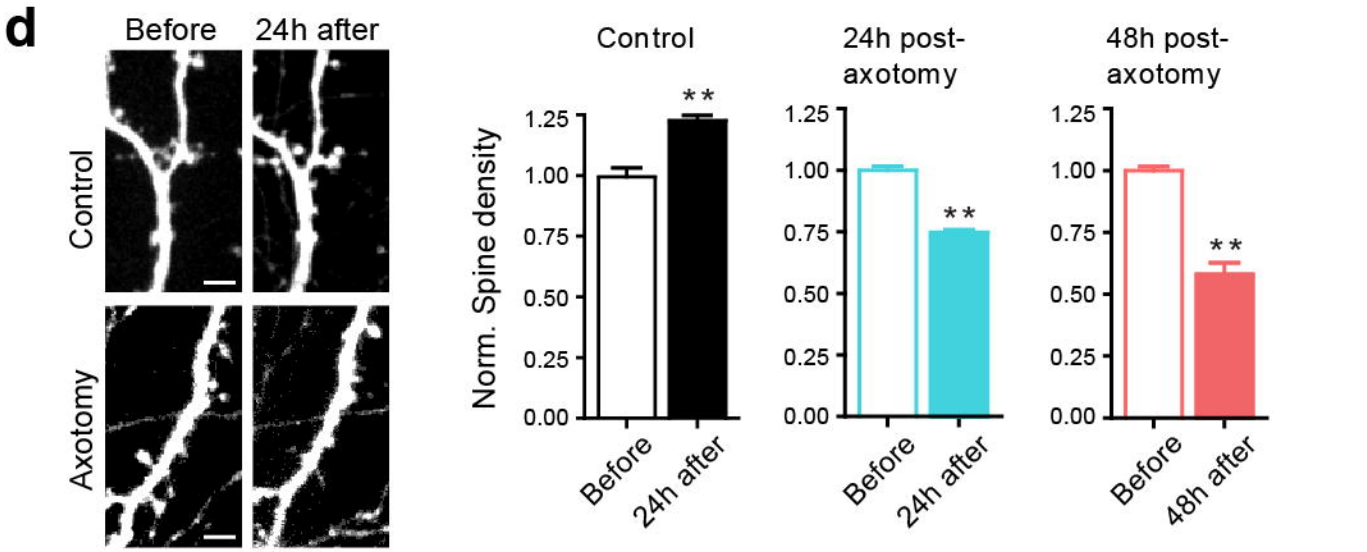


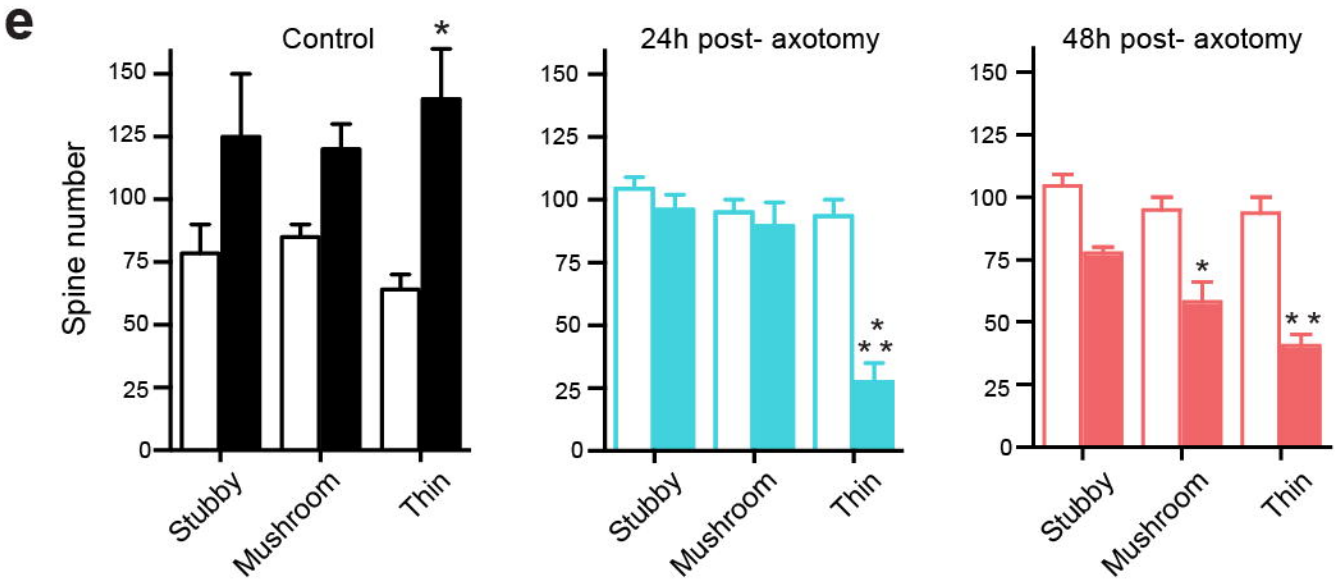


Fig. 1

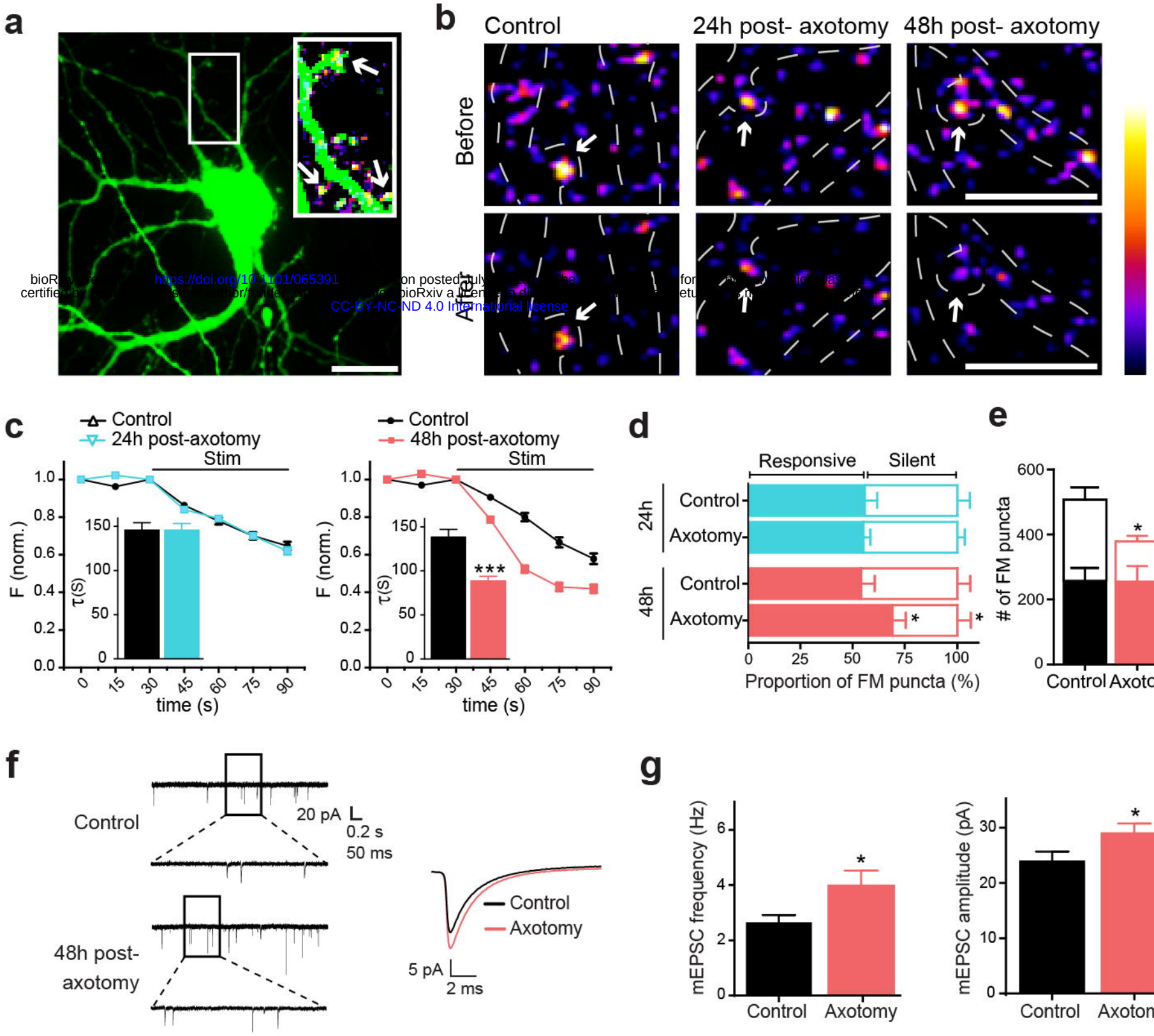


Fig. 2

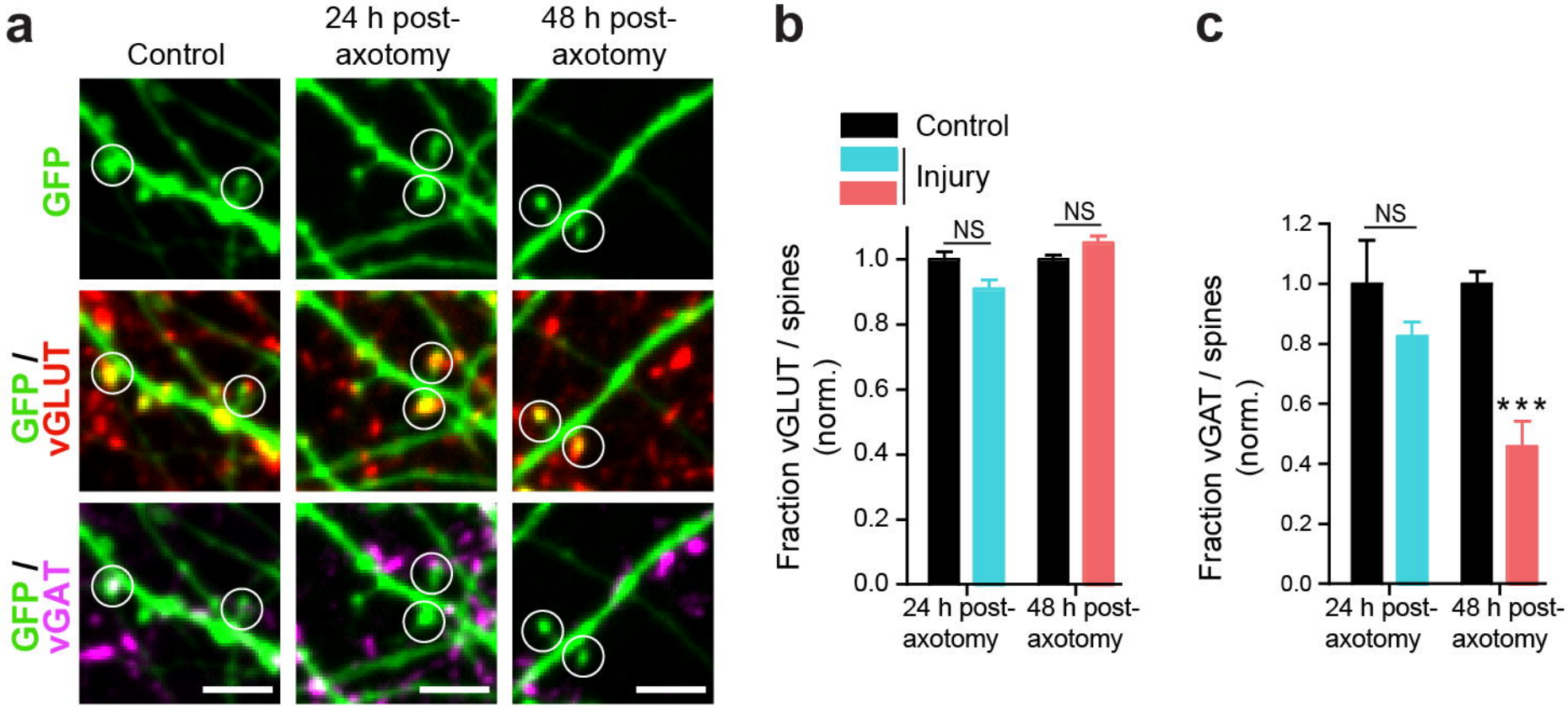
a
Control
24 h post-axotomy
48 h post-axotomy
GFP
GFP / vGLUT
GFP / vGAT
b
Control
Injury
NS
NS
Fraction vGLUT / spines (norm.)
1.0
0.8
0.6
0.4
0.2
0.0
24 h post-axotomy
48 h post-axotomy
c
NS
***
Fraction vGAT / spines (norm.)
1.2
1.0
0.8
0.6
0.4
0.2
0.0
24 h post-axotomy
48 h post-axotomy

Fig. 3

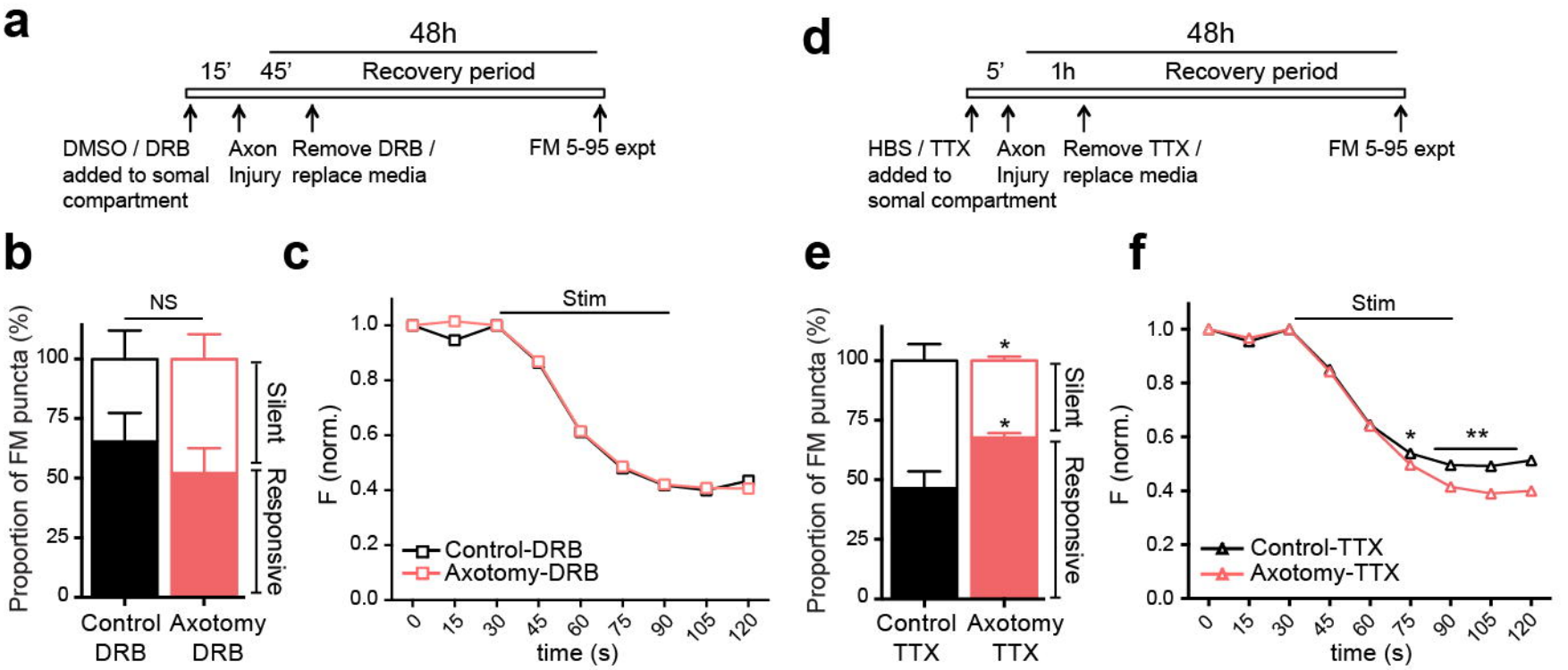
a
48h
15'
45'
Recovery period
DMSO / DRB added to somal compartment
Axon Injury
Remove DRB / replace media
FM 5-95 expt
d
48h
5'
1h
Recovery period
HBS / TTX added to somal compartment
Axon Injury
Remove TTX / replace media
FM 5-95 expt
b
NS
Proportion of FM puncta (%)
Silent
Responsive
Control DRB
Axotomy DRB
c
Stim
F (norm.)
Control-DRB
Axotomy-DRB
time (s)
e
Proportion of FM puncta (%)
Silent
Responsive
Control TTX
Axotomy TTX
f
Stim
F (norm.)
Control-TTX
Axotomy-TTX
time (s)

Fig. 4

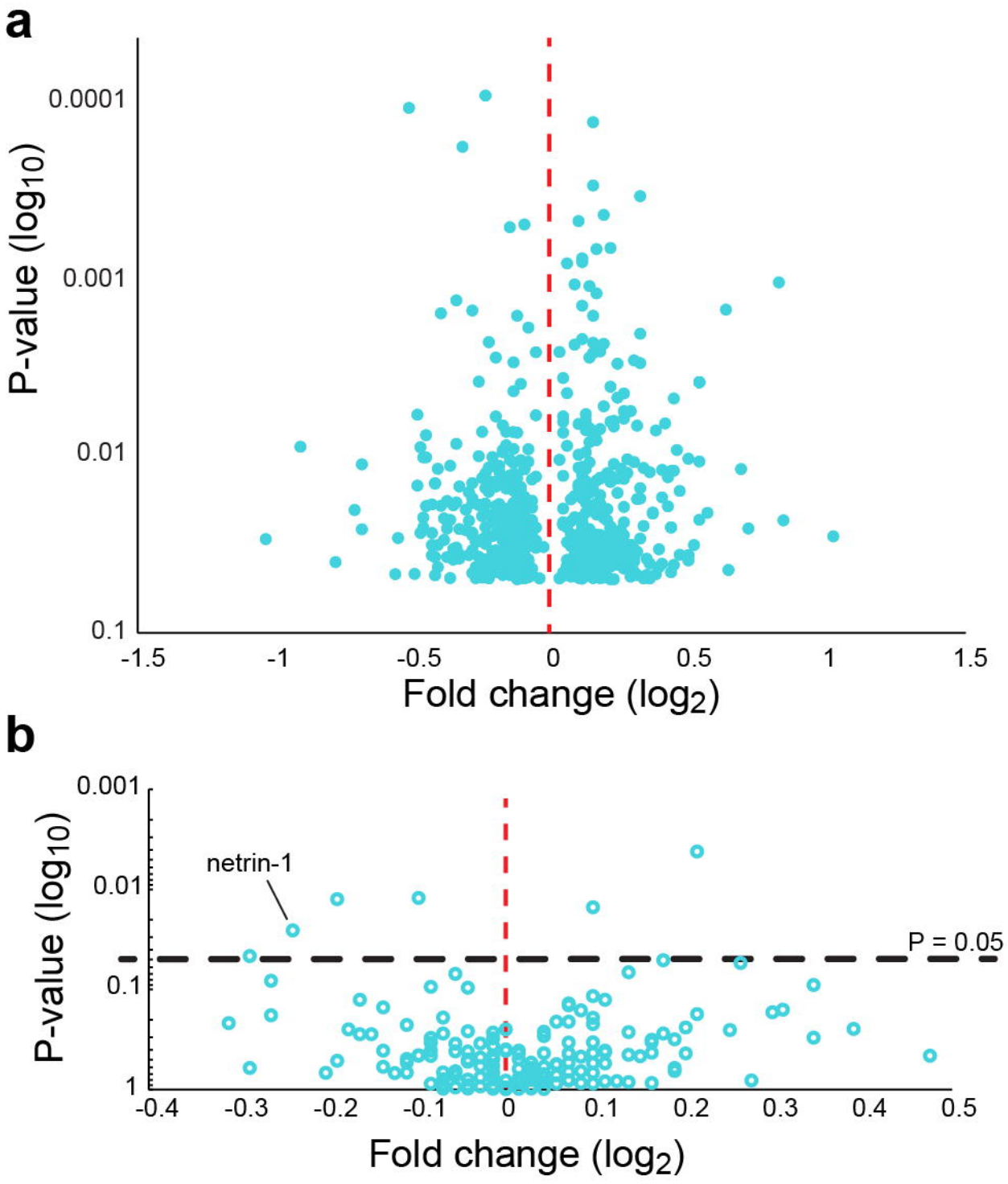


Fig. 5

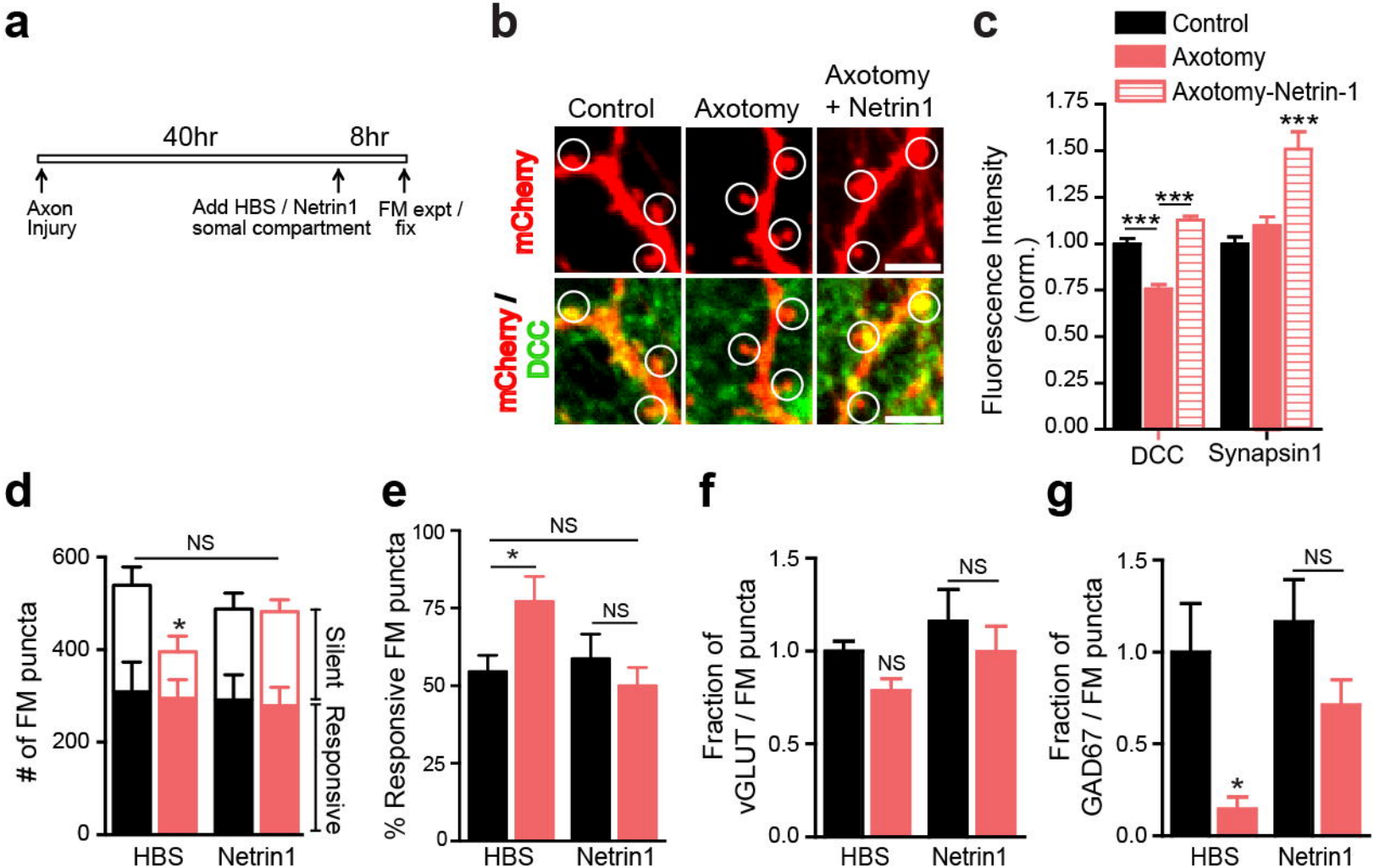
a
40hr
8hr
Axon Injury
Add HBS / Netrin1 somal compartment
FM expt / fix
b
Control
Axotomy
Axotomy + Netrin1
mCherry
mCherry / DCC
c
Control
Axotomy
Axotomy-Netrin-1
Fluorescence Intensity (norm.)
1.75
1.50
1.25
1.00
0.75
0.50
0.25
0.00
***
***
***
DCC
Synapsin1
d
# of FM puncta
600
400
200
0
NS
*
Silent
Responsive
HBS
Netrin1
e
% Responsive FM puncta
100
75
50
25
0
NS
*
NS
HBS
Netrin1
f
Fraction of vGLUT / FM puncta
1.5
1.0
0.5
0.0
NS
NS
HBS
Netrin1
g
Fraction of GAD67 / FM puncta
1.5
1.0
0.5
0.0
*
NS
HBS
Netrin1

Fig. 6